Macromolecular Research (2024) 32:1135–1144
https://doi.org/10.1007/s13233-024-00297-z

Online ISSN 2092-7673
Print ISSN 1598-5032

ARTICLE

Reduced migration of multi-arm structured plasticizer from pressure-sensitive adhesive films

Misol Kim[1] · Yun Jung Jang[2,3] · Yeonhee Lee[3] · Chaelim Mun[1] · Hanki Cho[4] · Hyunjee Yoo[4] · Jaseung Koo[1]

Received: 18 April 2024 / Revised: 24 June 2024 / Accepted: 27 June 2024 / Published online: 23 July 2024

Abstract

Temporary protective film (TPF) is used as a surface protection for the encapsulation layer during cell cutting and laser lift-off in the manufacturing process of an organic light-emitting diode. TPFs should satisfy the following requirements: good wettability on the surface during the protection step, low peel strength, and clear debonding properties during the removal step. Herein, we used multi-arm-structured trimethylolpropane ethoxylate (TPEG) and linear-structured poly(ethylene glycol) 200 (PEG200) plasticizers to attain these requirements for a polyurethane-based a pressure-sensitive adhesive (PSA). The PSA films with TPEG successfully satisfied the aforementioned requirements. The PSA films with plasticizers exhibited similar wettability and polar surface energy with those of the substrate, thereby demonstrating an interface energy with the substrate of approximately zero. Additionally, the 180° peel strength test showed that the peel strength of the PSA with TPEG was lower than that with PEG200. The observation coincides with small-amplitude oscillatory shear test results obtained via rotational rheology measurements. Furthermore, debonding properties were characterized using time-of-flight secondary ion mass spectrometry (TOF–SIMS) of the adherend surfaces after peeling off the TPFs. The structural properties of TPEG affected migration to a lesser extent than those of PEG200. This is in good agreement with the surface free energies of the adherend surfaces after removing the TPFs. The proposed design strategy can be applied in electronic industry where surface protection using ultra-peelable adhesive films is required.

Graphical abstract

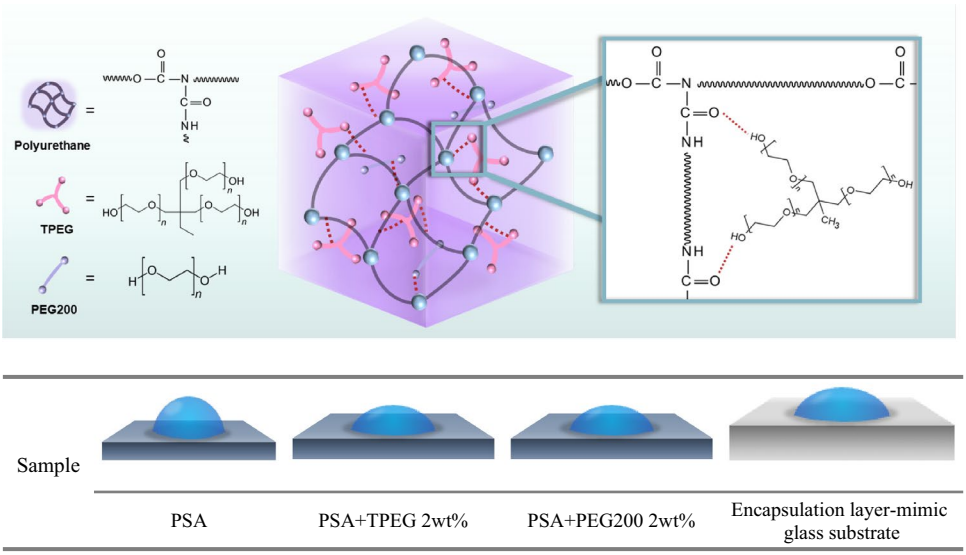

A schematic diagram of a thermally crosslinked urethane PSA with two plasticizer additives: multi-arm TPEG and linear PEG200. The addition of plasticizers forms hydrogen bonds with the polyurethane main chain

Extended author information available on the last page of the article

Keywords Pressure-sensitive adhesive · Temporary protective film · Plasticizer · TOF–SIMS

1 Introduction

Recently, the OLED display applications have been growing rapidly in the field of mobile devices and large television panels because of advanced developments through thin, flexible, and foldable device technologies [1–4]. PSA films are essential in the OLED display to cover, bond, and temporarily protect the surfaces between panels. A PSA film is defined as a thin, flexible tape with a single- or double-sided coating that is capable of bonding two disparate surfaces by applying slight pressure at room temperature without any chemical reaction [5, 6]. Additionally, the PSA film can be classified according to the peel strength. A removable PSA film refers to a PSA possessing the peel strength below 4 N/m, and the TPF belongs to this category [7–10].

TPF is used in the display to cover the top layer of the thin film encapsulation, which acts as a barrier layer for OLED devices [11–16]. It is temporarily used to protect the surface of the OLED encapsulation layer during processing and subsequently removed. The removal should be clear to avoid any residual contamination from the TPF on the adherend surface, which may cause bubbles and delamination at the contaminated interface during the folding process of the final products [17, 18].

In applications related to semiconductor and display processes, such as dicing or cell cutting processes, it is essential to evaluate presence and amount of PSA residues by surface analysis of the adherend after TPF is removed upon completion of the protection step. Previous studies of temporary bonding PSA used a scanning electron microscope (SEM), laser surface inspector and X-ray photoelectron spectroscopy (XPS) analyzing techniques to measure the PSA residues [19–23]. However, although SEM enables measuring the morphology of the adherend and residue distribution, SEM provides only information that can determine the presence or absence of residue. The laser surface inspector has limitations in measuring the amounts of residues accurately and quantitatively, and has a problem in that analysis of their components is impossible. Atomic elemental analysis of the residue is possible with XPS, but there is a limitation, in that it is not possible to know from which substances in the adhesive the elements were detected. To overcome these analytical limitations, we employed the TOF–SIMS technique to determine the location of residues remaining on the surface to be bonded and the cause of contamination by identifying the remaining materials.

The components of a PSA include main resins, crosslinkers, plasticizers, tackifiers, stabilizers, etc. [24]. Among these components, the plasticizers change the mechanical properties, such as flexibility and adhesion, of polymer resin films by forming secondary bonds between the plasticizer and polymer chains, thereby reducing the bonds between the polymer chains [25]. Among the various types of plasticizers, such as phthalate, benzoate, adipate, citrate, and polyol [26–32], polyethylene glycol (PEG)-based plasticizers have the advantage of increasing wettability while maintaining low peel strength [24].

In this study, we investigated the effect of molecular structure of plasticizers on the wettability, rheological, and mechanical properties of adhesives. Specifically, a multi-arm-structured TPEG and linear-structured PEG200 plasticizers were used to investigate the effect of the molecular structure of the plasticizer on residue migration. The contact angle measurements, the 180° peel strength tests, and the TOF–SIMS technique were employed to examine whether the PSA films met the three requirements for TPFs, namely good wettability, low peel strength, and minimum migration (Fig. 1).

2 Experimental section

2.1 Materials

Urethane adhesive solution and diisocyanate (OFLEX, Dajeon, Republic of Korea) were used as the main resin and thermal crosslinker, respectively. Trimethylolpropane ethoxylate, TPEG (Molecular weight $M_w = 450$), and polyethylene glycol, PEG200 ($M_w = 200$) (Sigma Aldrich, Darmstadt, Germany) were used as plasticizers. Silicone release film (50 μm thickness) and primer-coated PET films (125 μm thickness) were purchased from SKC, Korea.

2.2 Preparation of urethane PSA films

A thermal-curable urethane PSA resin was prepared by blending a urethane adhesive solution with a thermal crosslinker (7 wt%) and plasticizers (2 wt%). The PSA resin was mixed at 400 rpm for 20 min using a mechanical overhead stirrer (RW 20 digital, IKA, Staufen, Germany). Subsequently, the PSA resin was coated on the base film to a thickness of 35 μm at a speed of 33.4 mm/min using a knife-coating device (KP-3000VH, KIPAE, Korea). The coated films were heated at 120 °C for 2 min 30 s. Subsequently, the coated TPF samples were laminated with silicone release

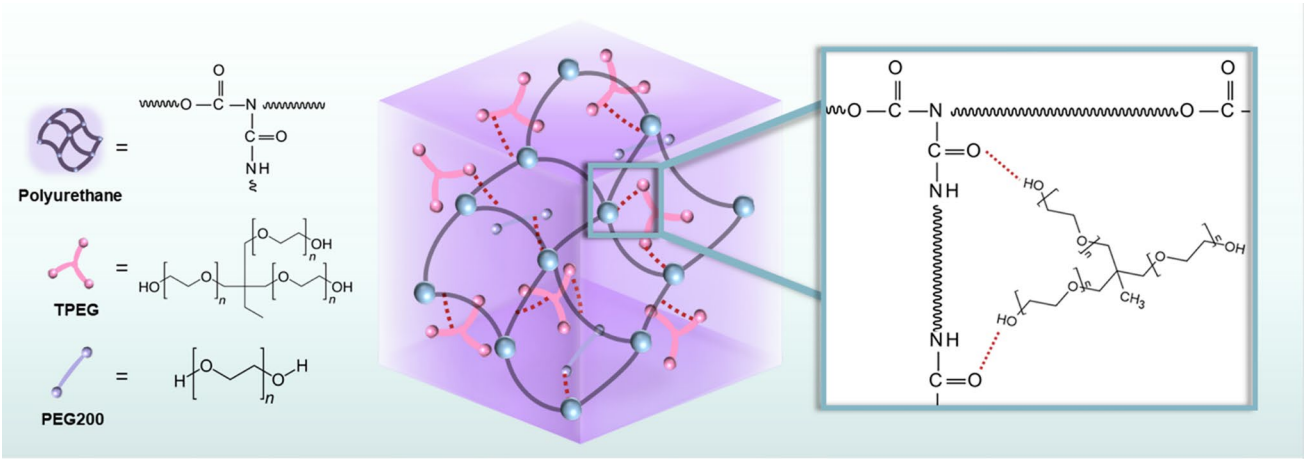

Fig. 1 **a** Schematic illustration of thermally crosslinked urethane PSA with two different plasticizer additives, i.e., multi-arm TPEG and linear PEG200. **b** Three main requirements for temporary protective PSA: improving the wettability of the adhesive to attach on uneven surface, minimizing the migration after peeling off, and reducing the peel strength to prevent surface damage

films using a laminator (EXCELAM II-355Q, GMP, Korea) and aged at 40 °C for 3 days.

2.3 Gel fraction

The gel fractions of urethane PSA films with and without plasticizers were determined by immersing 1 g of the sample wrapped in a wire mesh in toluene at 25 ℃ for 2 days to remove the non-crosslinked parts. After drying at 40 ℃, the gel fraction was calculated from gel content $(\%) = (W_1/W_0) \times 100$ where W_0 is the initial weight of the sample (mg), and W_1 is the solvent-extracted weight (mg).

2.4 Surface free energy

The surface free energy was calculated through contact angle measurements using polar and non-polar liquids, such as deionized (DI) water, ethylene glycol, formamide, and diiodomethane. The liquid drops were gradually placed on the adherend and PSA film. The contact angle (θ) was measured at 25 ℃ for 30 s with an interval of 0.5 s using a drop shape analyzer (DSA100, KRÜSS, Hamburg, Germany). This process was repeated ten times to determine the accurate mean value of the contact angle. The surface energy values were calculated using the Owens–Wendt–Rabel–Kaelble (OWRK) equation (see Supporting Information for details). The liquid drops were gradually placed on the adherend and PSA film. The contact angle (θ) was measured at 25 ℃ for 30 s with an interval of 0.5 s using a drop shape analyzer (DSA100, KRÜSS, Hamburg, Germany). This process was repeated ten times to determine the accurate mean value of the contact angle. The surface energy values were calculated using the OWRK equation (see Supporting Information for details).

2.5 Peel strength

The 180° peel strength tests (ASTM D3330) were performed using a universal testing machine (UTM AGS-5GX, Shimadzu, Kyoto, Japan). The PSA films were deposited on the encapsulation layer-mimic glass substrate using 2 kg hand rollers. After 24 h, the films were peeled off in the 180° direction at a speed of 300 mm/min.

2.6 Rheological measurements

The rheological and viscoelastic properties of the PSA films were determined using a rheometer (MCR 102e, Anton Paar, Graz, Austria). The storage (G') and loss (G'') moduli of PSA films were evaluated as a function of the concentration of TPEG and PEG200 used as a plasticizer. PSA films (thickness: 0.95–1.05 mm) were transferred to a parallel-plate fixture with a diameter of 8 mm. The samples were pressed in the form of disks between the parallel plates with a gap up to a force of 1 N. The strain sweep test was performed by increasing the shear strain from 0.01 to 10%. The samples were maintained at 25 °C and a constant angular frequency of 10 rad/s. The linear viscoelastic region (LVR) of each sample was determined. The frequency sweep test for small-amplitude oscillatory shear (SAOS) was performed by oscillating the samples over a range of frequencies from 0.1 to 100 rad/s with a monitored shear strain of 0.1% within the LVR at a constant temperature of 25 °C.

2.7 Instruments

Fourier-transform infrared (FT-IR) spectra were measured in the range of 4000–400 cm^{-1}, using the FT-IR spectroscopy (Alpha-P, Brucker, Germany). SiC glow bar source,

ZnSe beam splitter, and KBr/DLaTGS detector were used to provide a spectral resolution of 0.9 cm^{-1}. The samples were prepared with attached TPFs on encapsulation layer-mimic glass substrates for 24 h. TOF–SIMS spectra and two-dimensional (2D) images of the substrates with peeled-off TPFs were obtained using TOF–SIMS 5 (IONTOF, Münster, Germany) with a 30 keV Bi^{3+} primary ion beam in the high current bunched mode. The analysis current was kept at a pulsed current of 0.3 pA with a raster size of 100 × 100 µm, and the measured mass resolution was 5000 for m/z 29 Si peak for positive ion mode. The morphological structures of residues of the PSA specimens were characterized by scanning electron microscope (SEM, TESCAN, CLARA, Brno, Czech Republic) at an operation voltage of 1 kV. The energy-dispersive X-ray spectroscopy (EDS, Oxford Instruments, Ultim Max, Abingdon, Oxfordshire) of selected areas was conducted for elemental distribution analysis.

3 Results and discussion

3.1 FT-IR

The FT-IR spectroscopy (Fig. 2) shows evidence of the cross-linking of the PSA films with or without plasticizers. After the heat treatment and aging process, the spectra exhibit amide bond peaks (N–H stretching at 3360 cm^{-1}, N–H bending at 1527 cm^{-1}, and C=O stretching at 1724 cm^{-1}), which is an indication of cross-linking. Furthermore, the peaks of the isocyanate bond disappear in the spectra of PSA, PSA + TPEG, and PSA + PEG200 (e.g., NCO stretching at 2259 cm^{-1}) after heat treatment and aging, thereby suggesting the participation of all isocyanate groups in thermal cross-linking.

3.2 Wettability of TPFs

The surface free energy of the adhesive film is a significant factor in developing an adhesive force on the adherend. TPF with low wettability does not adhere well and causes slippage during its processing on the substrate. We added TPEG and PEG200 plasticizers in PSA films to improve the wettability of TPFs. The hydroxyl group at the end of the PEG forms a hydrogen bond with the urethane group, thereby improving the wettability [31, 33].

The surface energy was quantified using contact angle measurements to confirm the effect of imparting hydrophilicity (Table S1). Four different solvents, i.e., (diiodomethane, ethylene glycol, formamide, and DI water), were used to measure their respective contact angles on the surfaces of the TPFs film surfaces using the sessile drop method and to calculate the surface energy of the adhesive surfaces [34–36].

The contact angles of the polar and non-polar solvents on the PSA film, PSA film with TPEG (PSA + TPEG), PSA film with PEG200 plasticizers (PSA + PEG200), and a clear glass

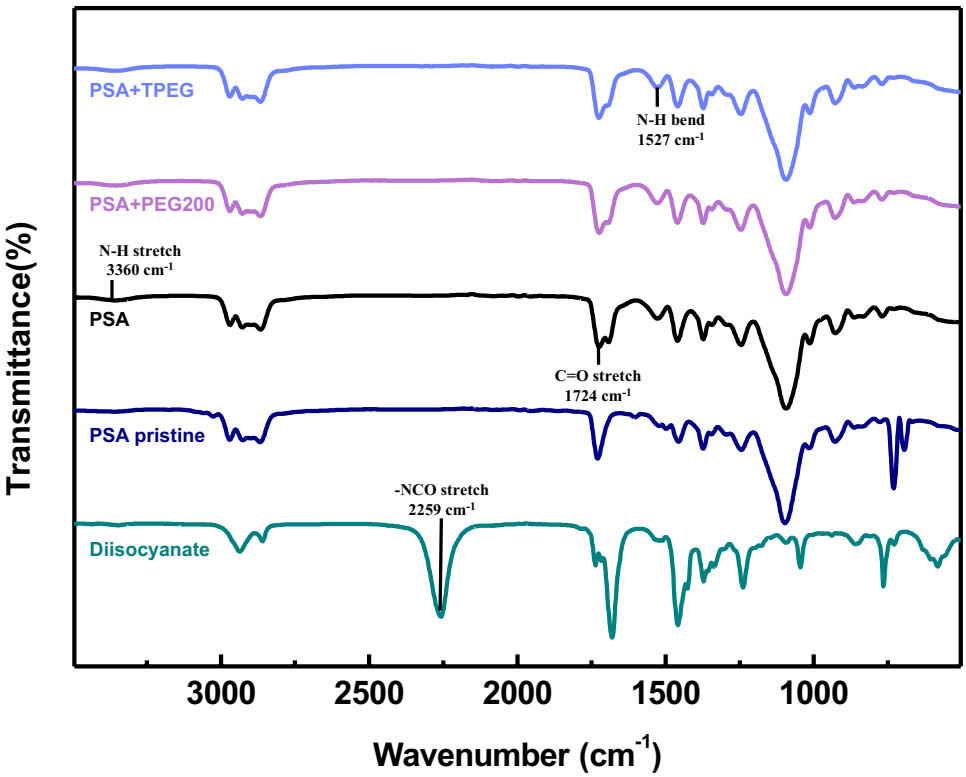

Fig. 2 FT-IR spectroscopy of PSA + TPEG, PSA + PEG200 and PSA after curing and aging, compared with Diisocyanate. Amide bond peaks (N–H stretching at 3360 cm^{-1}, N–H bending at 1527 cm^{-1}, and C=O stretching at 1724 cm^{-1}) indicates the formation of a cross-linking bond. NCO stretching at 2259 cm^{-1} indicates that all diisocyanates participated in the reaction

substrate are listed in Table 1. The solid surface energy (γ_s) is the sum of the components corresponding to the dispersion forces (γ^d) and polar forces (γ^p) as given in equation: $\gamma_s = \gamma^d + \gamma^p$ [37].

The interfacial energy $(\gamma_{\alpha\beta})$ between the two surfaces α and β is expressed in terms of the dispersion and polar forces for each phase as shown in equation: $\gamma_{\alpha\beta} = \gamma_\alpha + \gamma_\beta - 2\sqrt{\gamma_\alpha^d \gamma_\beta^d} - 2\sqrt{\gamma_\alpha^p \gamma_\beta^p}$ [37].

Pristine urethane TPFs have a lower polar surface energy than the encapsulation layer-mimicking glass substrate. When TPEG 2 wt% or PEG200 2 wt% was added, the water contact angle on the surface of the adhesive decreased by more than 20°. Consequently, the polar surface energy of the PSA with plasticizers increased more than 15% than that of the pristine urethane PSA. The polarity was also observed similar to that of the encapsulation layer-mimicking glass substrate. The interfacial energy between the adhesive film and substrate was calculated to deduce the adhesion mechanism. The pristine urethane PSA has an interfacial energy of 2 mN/m, both PSA + TPEG and PSA + PEG200 have low interfacial energies of 0mN/m as presented in Table 1. A decrease in the interfacial energy corresponds to an increase in wettability.

3.3 Peel strength of TPFs

PSA films were manufactured using urethane resin and a diisocyanate crosslinker. The peel strength was investigated with respect to the curing temperature and the presence or absence of aging of the urethane resin as shown in Fig. 3a. The neat samples (before aging) were heated for 2 min 30 s at different curing temperatures of 80, 100, 120, 140, and 160 °C. The aging samples were prepared by treating the previously synthesized PSA films for 3 days at 40 °C. The samples (neat) exhibited an unstable adhesive force of 412 and 152 mN/m at curing temperatures of 80 and 100 °C. The PSA films were not fully crosslinked, thereby resulting in a loss of cohesion and a sticky residue on the surface of the substrate. Furthermore, crosslinking failure decreased the cohesion and increased the

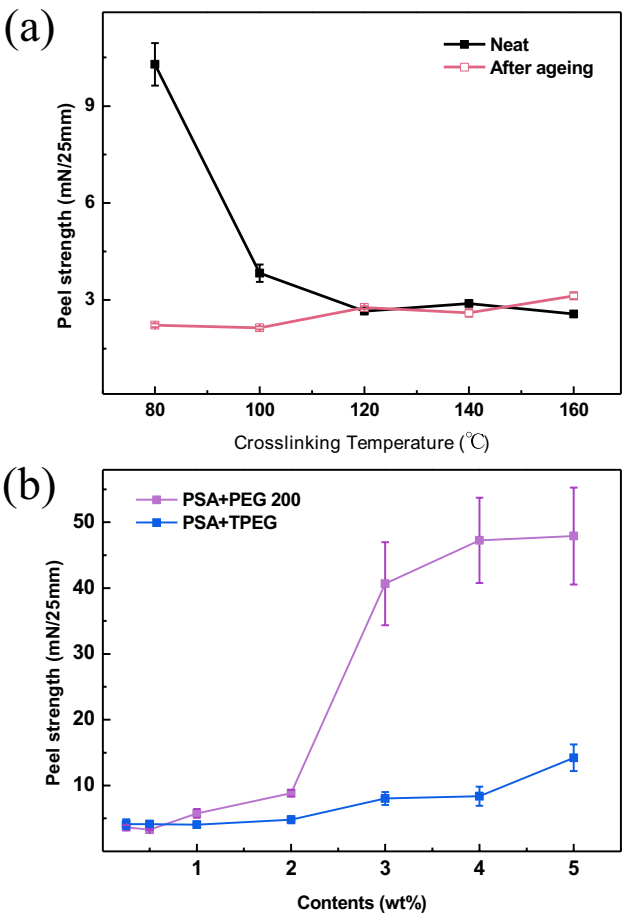

Fig. 3 Peel strength of **a** TPFs with and without aging after curing at the various cross-linking temperature. **b** 180° peel strength of TPFs after curing at 120 °C with various amounts of PEG200 and TPEG

Table 1 The surface free energy (γ_s) results of the adhesive surface (PSA, PSA + TPEG, PSA + PEG200) and the glass substrate

Sample	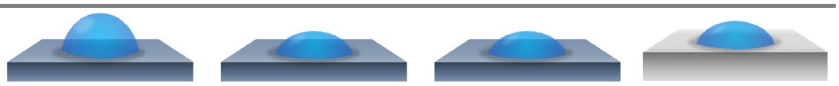			
	PSA	PSA+TPEG 2wt%	PSA+PEG200 2wt%	Encapsulation layer-mimic glass substrate
γ_s	37 mN/m	47 mN/m	43 mN/m	41 mN/m
γd	35 mN/m	33 mN/m	30 mN/m	31 mN/m
γ_p	3 mN/m	14 mN/m	13 mN/m	10 mN/m
$\gamma_{\alpha,\beta}$	2 mN/m	0 mN/m	0 mN/m	-

Calculation of the interfacial energy $(\gamma_{\alpha\beta})$ between the adhesive and adherend

peel strength during the debonding process. Peel strength is higher before cross-linking than after cross-linking. This is because, before cross-linking, there are more functional groups available to interact with the substrate surface compared to after cross-linking. Gel fractionation experiments were performed on the same samples to confirm these findings. The results are summarized in Table S3. The gel content of the samples is approximately 1% when the curing temperature is below 120 °C (Table S3(a)). At 80 and 100 °C, the neat samples are not fully crosslinked, thereby contributing to the increase in adhesion (Fig. 3a). Conversely, the aged samples have a peel strength of less than 160 mN/m at all curing temperatures. When aging is performed at 40 °C for 3 days, the cross-linking density improves, and peel strengths of the PSA films decrease. The gel content is 97% or higher at all temperatures (Table S3(b)), indicating that most of the uncured resin has been crosslinked. The gel fraction and the 180° peel test results suggest that the optimum curing temperature is 120 °C in this study.

Further, results of the peel tests were used to investigate the relationship between the adhesive properties of the wettability-improving plasticizers in the urethane resin and those of the pristine urethane resin as shown in Fig. 3b. The peel strength was tested by adding PEG200 or TPEG to the urethane PSA at concentrations of 0.25, 0.5, 1, 2, 3, 4, and 5 wt%. The chemical structure and the concentration of the plasticizer in an ultra-peelable pressure-sensitive adhesive have a significant impact on the peel adhesion. The peel strength of PSA + PEG200-2wt% and PSA + TPEG-2wt% slightly increases to 352 and 192 mN/m, respectively (Fig. 3b)). Additionally, the gel fraction experiments were performed on the same samples. The gel fractions decreased to 91.5% and 95.9%, respectively, compared to the PSA gel fraction of 96.5%. (Table S3(c)). When a plasticizer forms hydrogen bonds with the urethane group, the number of interacting hydroxyl groups in the PSA increases. It causes decrease of hydroxyl groups that can react with substrates. The van der Waals and the hydrogen bonds with the Si–O group result in a change in the peel strength [37]. Plasticizers increase the mobility of the polymer chains, which reduces peel strength. The addition of plasticizers allows the polymer chains to move freely, reducing the bond strength of the adhesive. The increased flexibility allows the adhesive to better conform to the substrate surface and distribute the applied stresses more evenly, allowing it to better absorb and manage mechanical stresses during peel testing, thereby reducing peel strength. Therefore, when the concentration of the plasticizers is increased, the urethane resin with TPEG shows lower peel strength than that with PEG200 at the same plasticizer concentration.

3.4 Rheology of TPFs

Rheological measurements of the PSA with TPEG and PEG200 were performed at 25 °C to compare with the peel strength results. Strain sweep and frequency sweep modes were applied to determine G' and G'' of PSA with different concentration (2 and 5 wt%) of TPEG or PEG200. In Fig. 4a, b, the strain sweep results show the typical linear (strain (γ) = 0.001–1%) and non-linear behavior (γ = 1–10%) of G'. A frequency sweep test was performed at 0.1% strain in the LVR of the strain sweep results. The measured G' for all samples in the frequency sweep is higher than the G'' in the measured frequency range (Fig. 4c, d). This suggests that the elastic properties are dominant, indicating sufficient chemical cross-linking in all the samples. Furthermore, the G'' values increase with increasing concentration of plasticizer in the PSA film. The observation is more pronounced in PSA with PEG200 than that with TPEG. This indicates that PEG200 softens the hard properties of the main chain, which is in good agreement with the higher peel strength and lower T_g value (Figure S2). Hence, we conclude that the PSA + TPEG maintains rigid behavior, thereby facilitating clear debonding during the TPF process [38].

3.5 Characterization of surface contamination

We employed the TOF–SIMS to detect and identify trace species on the surface [39–46]. TOF–SIMS 2D imaging technique was used to examine the residue on the encapsulation layer-mimicking glass substrate. TOF–SIMS operates by irradiating a sample surface with a primary ion beam (e.g., Ga^+, Bi^+, Cs^+), causing surface atoms and molecules to be emitted as secondary ions. These secondary ions are accelerated through an electric field, and their travel speed varies based on their mass. The time each ion takes to reach the detector is measured, allowing the calculation of the mass-to-charge ratio (m/z). Larger ions travel slower and smaller ions travel faster, resulting in different detection times and creating a mass spectrum. This technique enables the analysis of surface chemical composition at the nanometer level. Figure 5a, b shows the TOF–SIMS spectra of the surface of the glass-based adherend after peeling off the PSA + TPEG and PSA + PEG200, respectively. Peaks of organic compounds, such as $C_2H_3O^+$, $C_2H_4O^+$, $C_2H_5O^+$, and $C_3H_7O^+$, are observed in both the spectra. These peaks are also observed in the TOF–SIMS spectra of pure TPEG and PEG200 (Figure S1). The TOF–SIMS 2D imaging of $C_2H_5O^+$ and Si^+ ions for PSA + TPEG and PSA + PEG200 was used to compare the relative amounts of residues as shown in Fig. 5c. $C_2H_5O^+$ normalized by Si^+ images was obtained by dividing the $C_2H_5O^+$ intensity by the Si^+ intensity from pixel to pixel.

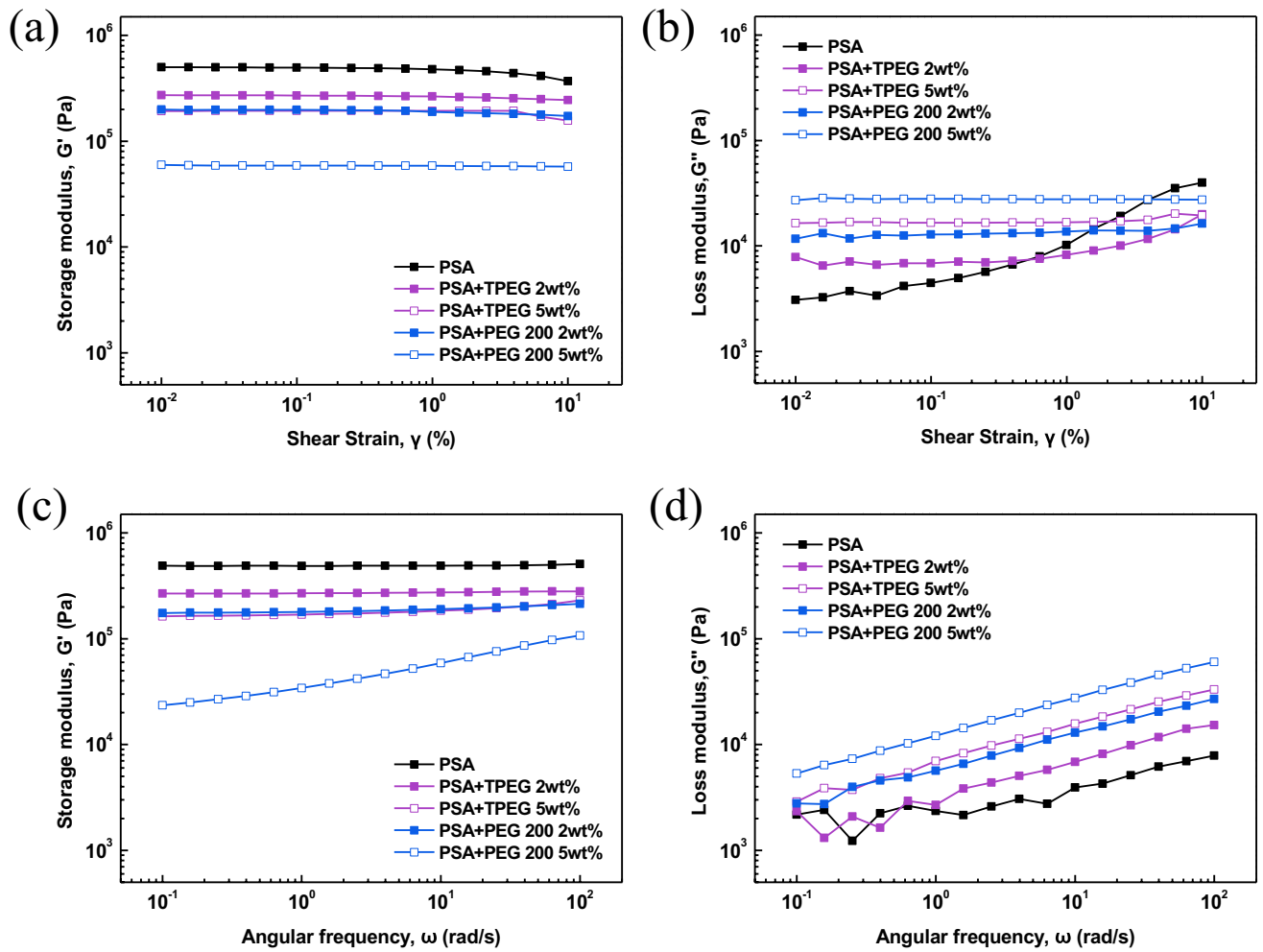

Fig. 4 **a** G' and **b** G'' of PSA with different weight ratio of TPEG (2 wt%, 5 wt%) and PEG200 (2 wt%, 5 wt%) at constant angular frequency of 10 rad/s and small shear strain region 0.01–10% **c** G' and **d** G'' of PSA with different weight ratio of TPEG (2 wt%, 5 wt%) and PEG200 (2 wt%, 5 wt%) with 0.1% shear strain at angular frequency region from 0.1 to 100 rad/s

The total count (TC) represents the sum of ions detected on a 2D TOF–SIMS given image. The TC of $C_2H_5O^+$ for PSA + TPEG (5.15×10^2) is observed lesser than that for PSA + PEG200 (7.36×10^2). Therefore, the surface of the glass-based adherend is more exposed, and the image intensity for Si^+ ions is 1.6 times stronger in PSA + TPEG (TC: 1.36×10^3) than those in PSA + PEG200 (TC: 8.49×10^2). The $C_2H_5O^+$ images normalized by Si^+ images of the PSA + TPEG show lower ion detection than that of the PSA + PEG200, thereby suggesting that TPF with TPEG is beneficial for maintaining low migration. One should notice that we can compare relative amounts of resides by other approaches, for example, contact angle and SEM measurements of adherend surfaces after peeling in Figure S2 and S3. However, in both cases, one cannot identify the residue molecules. Only 2D TOF–SIMS technique enables determining the relative amount of residue and identify the residue composition at the same time.

The difference in migration is due to the discrepancy in the diffusion dynamics of TPEG and PEG200 in the matrix. TPEG and PEG200 have the same chemical compound, i.e., ethylene glycol; however, they have different molecular architectures: the star structure of TPEG and the linear structure of PEG200. The hydrophilic PEG200 tends to diffuse into the hydrophilic encapsulation layer-mimicking glass surface [47]. Conversely, the three arms of the star-shaped TPEG plasticizer form an entanglement with the matrix polymer. Thus, the branch point of the star polymer is anchored in the urethane main chain network, showing a significantly lower diffusion behavior than that of the linear polymer [48]. These dynamic properties provide the advantage of significantly low migration of star-structured TPEG, thereby allowing the design of adhesive films with less residue during debonding process.

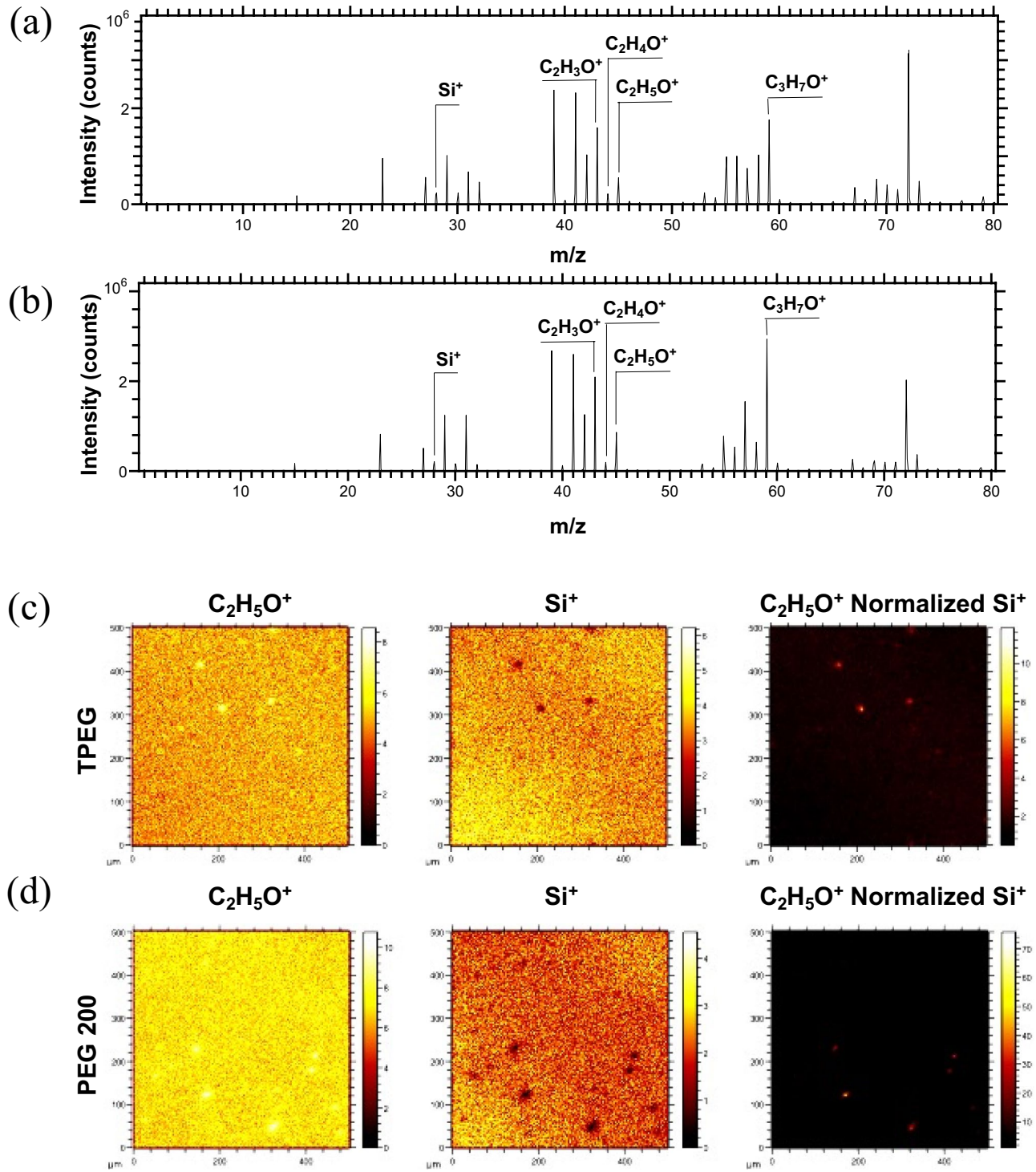

Fig. 5 TOF–SIMS spectra of $C_2H_5O^+$ and Si^+ ions from the surfaces of encapsulation layer-mimic adherends after peeling off PSA films with TPEG and PEG200 plasticizers, denoted as **a** PSA + TPEG and **b** PSA + PEG200, respectively. Corresponding TOF–SIMS 2D images **c** PSA + TPEG and **d** PSA + PEG200

4 Conclusion

We investigated the effect of the molecular structures of ethylene glycol-based plasticizers (linear-structured PEG200 and multi-arm-structured TPEG) on the major properties required for low-adhesive peelable PSA: (1) suitable wettability on the upper surface of the OLED, (2) low peel strength, and (3) minimal residue migration. The major

observations are summarized below: first, the interfacial energy between PSA layer and OLED surface-like substrate was reduced by more than 85% after adding PEG200 and TPEG, suggesting that the plasticizers provide suitable wetting properties to the PSA. Second, the peel strength of PSA + TPEG (192 mN/m) was approximately half than that of PSA + PEG200 (352 mN/m) at the same concentration of plasticizer. This is consistent with the rheological results. The loss modulus (G'') of PSA + TPEG increased owing to the softening effect of the plasticizer. However, the rigid behavior was maintained. Lastly, the TOF–SIMS results suggested that TPEG enabled clear debonding than PEG200. This is because the multi-arm structure of TPEG was anchored to the main chain, resulting in minimal migration. In general, when a low-molecular-weight polymer is added to the PSA, it increases adhesion and causes cohesive failure, which can result in residues on the surface [32]. TPEG could minimize the migration owing to its molecular structural characteristics. Therefore, we conclude that the multi-arm structure of TPEG functions adequately to develop a temporary protective material for the OLED manufacturing process and facilitates the three key characteristics that peelable PSA should possess: high wettability, low peel strength, and minimal migration.

Supplementary Information The online version contains supplementary material available at https://doi.org/10.1007/s13233-024-00297-z.

Acknowledgements This work was supported by research fund of Chungnam National University.

Declarations

Conflict of interest No potential conflict of interest was reported by the authors.

References

1. S. Park, W.M. Yun, L.H. Kim, S. Park, S.H. Kim, C.E. Park, Inorganic/organic multilayer passivation incorporating alternating stacks of organic/inorganic multilayers for long-term air-stable organic light-emitting diodes. Org. Electron. **14**, 3385–3391 (2013)
2. G. Crawford, *Flexible Flat Panel Displays* (Wiley, Oxford, 2005)
3. A.V. Pocius, D.A. Dillard, *Adhesion Science and Engineering: Surfaces, Chemistry and Applications* (Elsevier, Oxford, 2002)
4. C. Creton, Pressure-sensitive adhesives: an introductory course. Mater. Res. Soc. Newsl. Bull. **28**, 434–439 (2003)
5. Z. Czech, A. Kowalczyk, J. Swiderska, Pressure-sensitive adhesives for medical applications. Wide Spectra Qual. Control **17**, 310–332 (2011)
6. S. Mapari, S. Mestry, S. Mhaske, Developments in pressure-sensitive adhesives: a review. Polym. Bull. **78**, 4075–4108 (2021)
7. A.I. Everaerts, J.D. Malmer, Removable, low melt viscosity acrylic pressure sensitive adhesives. European Patent, No. EP0619831A1, (1996)
8. Z. Czech, Solvent-based pressure-sensitive adhesives for removable products. Int. J. Adhes. Adhes. **26**, 414–418 (2006)
9. C. Bandl, W. Kern, S. Schlögl, Adhesives for "debonding-on-demand": Triggered release mechanisms and typical applications. Int. J. Adhes. Adhes. **99**, 102585 (2020)
10. Z. Czech, A. Butwin, Development of photoreactive UV-crosslinkable solvent-free acrylic pressure-sensitive adhesives coated at room temperature and used for removable and repositionable self-adhesive materials. Pol. J. Chem. Technol. **13**, 31–34 (2011)
11. M. Eritt, C. May, K. Leo, M. Toerker, C. Radehaus, OLED manufacturing for large area lighting applications. Thin Solid Films **518**, 3042–3045 (2010)
12. S.H.K. Park, J. Oh, C.S. Hwang, J.I. Lee, Y.S. Yang, H.Y. Chu, K.Y. Kang, Ultra thin film encapsulation of organic light emitting diode on a plastic substrate. ETRI J. **27**, 545–550 (2005)
13. D. Yu, Y.-Q. Yang, Z. Chen, Y. Tao, Y.-F. Liu, Recent progress on thin-film encapsulation technologies for organic electronic devices. Opt. Commun. **362**, 43–49 (2016)
14. J.-S. Park, H. Chae, H.K. Chung, S.I. Lee, Thin film encapsulation for flexible AM-OLED: a review. Semicond. Sci. Technol. **26**, 034001 (2011)
15. E.G. Jeong, J.H. Kwon, K.S. Kang, S.Y. Jeong, K.C. Choi, A review of highly reliable flexible encapsulation technologies towards rollable and foldable OLEDs. J. Inf. Display **21**, 19–32 (2020)
16. J. Affinito, M. Gross, C. Coronado, G. Graff, I. Greenwell, P. Martin, A new method for fabricating transparent barrier layers. Thin Solid Films **290**, 63–67 (1996)
17. L. Zhang, Y. Cao, L. Wang, L. Shao, Y. Bai, Polyacrylate emulsion containing IBOMA for removable pressure sensitive adhesives, J. Appl. Polym. Sci., **133** (2016).
18. I. Benedek, M.M. Feldstein, *Applications of Pressure-Sensitive Products* (CRC Press, Boca Raton, 2008)
19. B. Sun, H. Wang, Y. Fan, X. Chu, S. Liu, S. Zhao, M. Zhao, Fully cross-linked UV-induced peelable acrylic PSA prepared from a dual curable castor oil based urethane acrylate oligomer for wafer dicing. Prog. Org. Coat. **163**, 106680 (2022)
20. P. Hao, B. Sun, X. Chu, Y. Sun, X. Xing, S. Liu, E. Tang, X. Xu, Effect of castor oil based urethane oligomer on properties of UV-curable pressure sensitive adhesive for peelable wafer dicing tape. J. Adhes. Sci. Technol. **34**, 2499–2509 (2020)
21. S.-W. Lee, J.-W. Park, H.-J. Kim, K.-M. Kim, H.-I. Kim, J.-M. Ryu, Adhesion performance and microscope morphology of UV-curable semi-interpenetrated dicing acrylic PSAs in Si-wafer manufacture process for MCP. J. Adhes. Sci. Technol. **26**, 317–329 (2012)
22. K. Ebe, H. Seno, K. Horigome, UV curable pressure-sensitive adhesives for fabricating semiconductors. I. Development of easily peelable dicing tapes. J. Appl. Polym. Sci. **90**, 436–441 (2003)
23. S.-W. Lee, J.-W. Park, C.-H. Park, D.-H. Lim, H.-J. Kim, J.-Y. Song, J.-H. Lee, UV-curing and thermal stability of dual curable urethane epoxy adhesives for temporary bonding in 3D multi-chip package process. Int. J. Adhes. Adhes. **44**, 138–143 (2013)
24. D.-H. Lim, H.-S. Do, H.-J. Kim, J.-S. Bang, G.-H. Yoon, Preparation of SIS/SBS-based UV-cross-linkable pressure-sensitive adhesives using the thiol-ene reaction. J. Adhes. Sci. Technol. **21**, 589–603 (2007)
25. A. Gal, A. Nussinovitch, Plasticizers in the manufacture of novel skin-bioadhesive patches. Int. J. Pharm. **370**, 103–109 (2009)
26. K.M. Shea, C.O.E. Health, Pediatric exposure and potential toxicity of phthalate plasticizers. Pediatrics **111**, 1467–1474 (2003)
27. M. Trends, A.D. Dave, S. Solutions, T. Talk, A. Store, I. Links, T.A. Tour, A. Index, Dibenzoate plasticizers in waterborne acrylic PSAs, (2014)
28. J. Gartshore, D.G. Cooper, J.A. Nicell, Biodegradation of plasticizers by *Rhodotorula rubra*. Environ. Toxicol. Chem. Int. J. **22**, 1244–1251 (2003)

29. M. Baiardo, G. Frisoni, M. Scandola, M. Rimelen, D. Lips, K. Ruffieux, E. Wintermantel, Thermal and mechanical properties of plasticized poly (L-lactic acid). J. Appl. Polym. Sci. **90**, 1731–1738 (2003)
30. S.D. Barhate, M. Patel, A.S. Sharma, P. Nerkar, G. Shankhpal, Formulation and evaluation of transdermal drug delivery system of carvedilol. J. Pharm. Res. **2**, 663–665 (2009)
31. S.F. Dana, D.-V. Nguyen, J.S. Kochhar, X.-Y. Liu, L. Kang, UV-curable pressure sensitive adhesive films: effects of biocompatible plasticizers on mechanical and adhesion properties. Soft Matter **9**, 6270–6281 (2013)
32. B. Ghanbarzadeh, M. Musavi, A. Oromiehie, K. Rezayi, E.R. Rad, J. Milani, Effect of plasticizing sugars on water vapor permeability, surface energy and microstructure properties of zein films. LWT-Food Sci. Technol. **40**, 1191–1197 (2007)
33. Y. Li, R. Zhang, H. Chen, J. Zhang, R. Suzuki, T. Ohdaira, M. Feldstein, Y. Jean, Depth profile of free volume in a mixture and copolymers of poly (N-vinyl-pyrrolidone) and poly (ethylene glycol) studied by positron annihilation spectroscopy. Biomacromol **4**, 1856–1864 (2003)
34. D.K. Owens, R. Wendt, Estimation of the surface free energy of polymers. J. Appl. Polym. Sci. **13**, 1741–1747 (1969)
35. D. Sowa, Z. Czech, Ł Byczyński, Peel adhesion of acrylic pressure-sensitive adhesives on selected substrates versus their surface energies. Int. J. Adhes. Adhes. **49**, 38–43 (2014)
36. F. Hejda, P. Solar, J. Kousal, Surface free energy determination by contact angle measurements–a comparison of various approaches. In: WDS, pp. 25–30 (2010)
37. P.C. Rieke, Application of Van Oss-Chaudhury-Good theory of wettability to interpretation of interfacial free energies of heterogeneous nucleation. J. Cryst. Growth **182**, 472–484 (1997)
38. T. Sartori, G. Feltre, P.J. do Amaral Sobral, R.L. da Cunha, F.C. Menegalli, Biodegradable pressure sensitive adhesives produced from vital wheat gluten: effect of glycerol as plasticizer. Colloids Surf A Physicochem Eng Asp **560**, 42–49 (2019)
39. M. Szynkowska, K. Czerski, J. Grams, T. Paryjczak, A. Parczewski, Preliminary studies using imaging mass spectrometry TOF-SIMS in detection and analysis of fingerprints. Imaging Sci. J. **55**, 180–187 (2007)
40. M.I. Szynkowska, A. Parczewski, K. Szajdak, J. Rogowski, Examination of gunshot residues transfer using ToF-SIMS. Surf. Interface Anal. **45**, 596–600 (2013)
41. P. Rostam-Khani, J. Philipsen, E. Jansen, H. Eberhard, P. Vullings, Quantitative analysis of surface contaminants on silicon wafers by means of TOF-SIMS. Appl. Surf. Sci. **252**, 7255–7257 (2006)
42. M. Szynkowska, K. Czerski, J. Rogowski, T. Paryjczak, A. Parczewski, Detection of exogenous contaminants of fingerprints using ToF-SIMS. Surf. Interface Anal. **42**, 393–397 (2010)
43. F. Zanderigo, S. Ferrari, G. Queirolo, C. Pello, M. Borgini, Quantitative TOF-SIMS analysis of metal contamination on silicon wafers. Mater. Sci. Eng. B **73**, 173–177 (2000)
44. K.L. Sek, P.L. Lee, K.Y. Pang, Y. Hua, L. Zhu, X. Li, Principal component analysis (PCA) of surface contamination by TOF-SIMS. In: 2021 IEEE International Symposium on the Physical and Failure Analysis of Integrated Circuits (IPFA), IEEE, pp. 1–4 (2021)
45. O. Dalby, D. Butler, J.W. Birkett, Analysis of gunshot residue and associated materials—a review. J. Forens. Sci. **55**, 924–943 (2010)
46. J. Coumbaros, K.P. Kirkbride, G. Klass, W. Skinner, Characterisation of 0.22 caliber rimfire gunshot residues by time-of-flight secondary ion mass spectrometry (TOF-SIMS): a preliminary study. Forens. Sci. Int. **119**, 72–81 (2001)
47. H.M. Said, N.G. Nik Salleh, M.S. Alias, A.W.M. El-Naggar, Synthesis and characterization of hard materials based on radiation cured bio-polymer and nanoparticles. J. Radiat. Res. Appl. Sci. **6**, 71–78 (2013)
48. M. Rubinstein, R.H. Colby, *Polymer Physics* (Oxford University Press, New York, 2003)

Authors and Affiliations

Misol Kim[1] · Yun Jung Jang[2,3] · Yeonhee Lee[3] · Chaelim Mun[1] · Hanki Cho[4] · Hyunjee Yoo[4] · Jaseung Koo[1]

✉ Jaseung Koo
jkoo@cnu.ac.kr

[1] Department of Organic Applied Materials Engineering, Chungnam National University, Daejeon 34134, Republic of Korea

[2] Advanced Analysis and Data Center, Korea Institute of Science and Technology, Seoul 02792, Korea

[3] Department of Materials Science and Engineering, Korea University, Seoul 02841, Korea

[4] R&D Center, O-Flex Co, Ltd., Daejeon 34025, Korea